Topography and refractometry of nanostructures using spatial light interference microscopy

Zhuo Wang,[1] Ik Su Chun,[1] Xiuling Li,[1] Zhun-Yong Ong,[2] Eric Pop,[1] Larry Millet,[3]
Martha Gillette,[3] and Gabriel Popescu[1,*]

[1]*Department of Electrical and Computer Engineering, Beckman Institute for Advanced Science and Technology,*
University of Illinois at Urbana-Champaign, Urbana, Illinois 61801, USA
[2]*Department of Physics, University of Illinois at Urbana-Champaign, Urbana, Illinois 61801, USA*
[3]*Department of Cell and Developmental Biology, University of Illinois at Urbana-Champaign, Urbana,*
Illinois 61801, USA
*Corresponding author: gpopescu@illinois.edu

Spatial light interference microscopy (SLIM) is a novel method developed in our laboratory that provides quantitative phase images of transparent structures with a 0.3 nm *spatial* and 0.03 nm *temporal* accuracy owing to the white light illumination and its common path interferometric geometry. We exploit these features and demonstrate SLIM's ability to perform topography at a single atomic layer in graphene. Further, using a decoupling procedure that we developed for cylindrical structures, we extract the axially averaged refractive index of semiconductor nanotubes and a neurite of a live hippocampal neuron in culture. We believe that this study will set the basis for novel high-throughput topography and refractometry of man-made and biological nanostructures. © 2010 Optical Society of America
OCIS codes: 180.3170, 120.5050.

Quantitative phase imaging (QPI) has recently become an active field of study and novel experimental approaches have been proposed to improve the existing (qualitative) phase contrast and differential contrast microscopy [1,2]. The range of QPI applications in biology has been broadened to cover red blood cell imaging [3], cell dry mass [4], cell and tissue refractometry [5], and polarization imaging [6]. Remarkably, due to the quantitative phase information rendered, the QPI is capable of bridging the fields of light scattering and imaging via Fourier transform light scattering, which is the spatial analog of Fourier transform spectroscopy [7].

However, because of speckle noise, QPI methods so far have not matched the resolving power of white light techniques such as phase contrast microscopy. To overcome this obstacle, we combined the QPI with a commercial phase contrast microscope, which uses white light illumination [8]. As a result, this method, referred to as spatial light interference microscopy (SLIM), is speckle free and, thus, exhibits a 0.29 nm optical-length sensitivity spatially (pixel to pixel), which significantly exceeds the performance of previously reported QPI systems. This allows nanoscale accuracy in thickness measurements if the refractive index is known and, conversely, highly accurate refractive index information if the thickness is known. In this Letter, we present for the first time, to our knowledge, a novel application of SLIM to graphene topography at the single atomic layer and refractometry of cylindrical structures, i.e., nanotubes and neurites.

SLIM is described in more detail elsewhere [8]. Briefly, the SLIM can be characterized as a combination of Zernike's phase contrast microscopy and Gabor's holography. SLIM was developed by producing additional spatial modulation to the image field outputted by a commercial phase contrast microscope. Specifically, in addition to the $\pi/2$ shift introduced in phase contrast microscopy between the scattered and unscattered light from the sample [9], we generated three additional phase steps, in increments of $\pi/2$, via a liquid crystal phase modulator. Four images corresponding to each phase shift were recorded and combined to produce a *quantitative phase image*.

To demonstrate the capability of SLIM for imaging single atomic layers, we first performed measurements on graphene flakes. Graphene is a two-dimensional lattice of hexagonally arranged and sp^2-bonded carbon atoms, i.e., a monolayer of the bulk material graphite. The graphene sample was obtained here by mechanically exfoliating a natural graphite crystal using an adhesive tape [10]. The exfoliated layers were deposited on a glass slide that was then cleaned using isopropanol and acetone to remove excess adhesive residues. Single-layer (graphene) and few-layer graphite flakes are routinely obtained in this process, with lateral dimensions of up to several tens of micrometers.

Figure 1(a) shows SLIM image of such a graphene flake. Qualitatively, it can be seen that the background noise is below the level of the sample itself. To quantify the nanoscale profile of this structure we transformed the phase distribution ϕ into thickness h, via $h = \phi\lambda/2\pi(n-1)$, with $n = 2.6$ being the refractive index of graphite [11]. Thus, we generated the topography histogram of the entire sample and individual regions as shown in Fig. 1(b). The overall histogram exhibits local maxima at topography values of 0 (background), 0.55, 1.1, and 1.65 nm. These results indicate that the topography of the graphene sample has a *staircase* profile, in increments of 0.55 nm. This is comparable with reported values in the literature for the thickness of *individual atomic layers* of graphene via atomic force microscopy (AFM) in air ($\sim$1 nm step size) or scanning tunneling micros-
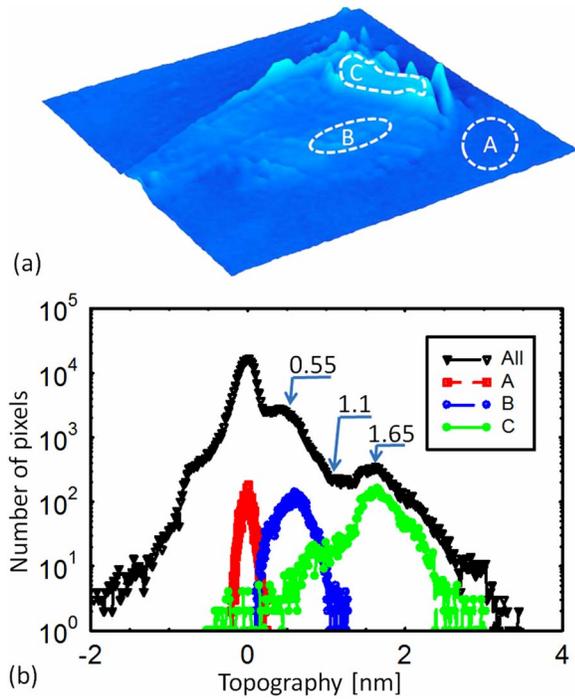
Fig. 1. (Color online) SLIM topography of graphene. (a) Quantitative phase image of a graphene flake. (b) Topography histogram for the various regions indicated in (a).

copy (STM) in ultrahigh vacuum (~0.4 nm step size) [12,13]. The difference between air and vacuum measurements indicates the presence of ambient species (nitrogen, oxygen, water, and organic molecules) on the graphene sheet in air. Thus, SLIM provides topographical accuracy that is comparable with the AFM, but its acquisition time is much faster (by 2–3 orders of magnitude) and, of course, it operates in a noncontact mode.

SLIM was further applied to image semiconductor nanotubes (SNTs). The SNT is a new type of nanotechnology building block [14]. It is formed by a combination of bottom-up and top-down approaches through self-rolling of residually strained thin films that are epitaxially grown and lithographically defined. The tube diameter is determined by the total layer thickness and the mismatch strain in the epitaxial layers (bottom-up aspect). The top-down aspect allows feasible large area assembly and integration with existing semiconductor technologies. Heterojunctions including structures with active light emitters embedded in the wall of the tube [14,15]. For this study, clusters of such rolled-up tubes consisting of InGaAs/GaAs coated with Cr/Au (see Fig. 2 for structure and SEM images) are randomly distributed on glass slides and imaged by SLIM.

Figures 2(e)–2(g) show the results of SLIM investigation of such nanotube structures. We used the prior knowledge of the tube cylindrical shape to decouple the thickness and the refractive index as demonstrated on the 15 μm $\times$ 20 μm SLIM image of Fig. 2(e). This procedure operates on the principle that the tube thickness, generally unknown, can be obtained for cylindrical structures from the projected width, which is directly measurable in the image. Of course, the refractive index information reports on
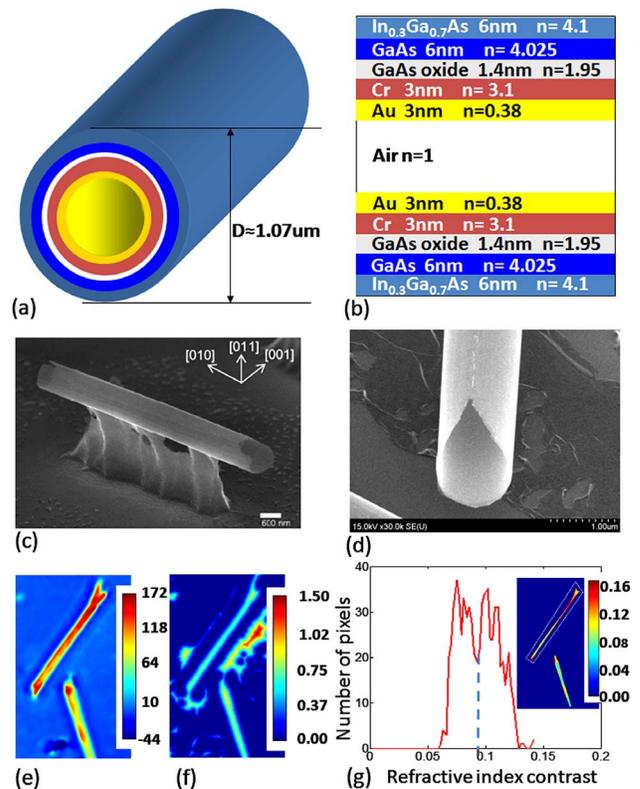

Fig. 2. (Color online) (a) Tube structure with refractive index and thickness of layers shown in (b). (c),(d) SEM images of nanotubes. (e) Optical path-length map; color bar is in nanometers. (f) Distance map; color bar is in micrometers. (g) Histogram of the refractive index contrast, $n-1$, of the selected area in the inset. Inset, distribution of refractive index contrast, $n-1$.

the chemical composition of the nanotube and its optical behavior. Using thresholding and binary masking of the SLIM image, we measured the distribution of the tube projected width, which is illustrated in Fig. 2(f). This *distance map* shows the distance from the center of the tube to its edge; thus the diameter is twice the number indicated by the color bar. This process was implemented via an automated routine in ImageJ, an image processing platform based on Java. Assuming that the tube thickness h and width are equal, we extracted the average tube refractive index, $(n-1) = \phi\lambda/2\pi h$. Note that for each tube SLIM provides refractive index information that is spatially resolved. Thus, in Fig. 2(g), we present the histogram of the refractive index measured along one of the nanotubes. The average value, $n_{av}-1 = 0.093$, compares very well with the estimated value, $n_{est} = 1.087$, resulted from averaging the refractive index for the layered structure shown in Fig. 2(b), $n_{est}^2 = (\Sigma_i n_i^2 h_i)/h$. The fluctuations in the refractive index along the nanotube are most likely due to physical inhomogeneities in the tube itself. We believe that SLIM may offer a high-throughput screening method for nanofabricated structures.

We employed this refractometry procedure to extract the refractive index of neuron processes, i.e., axons and dendrites, which are also characterized by cylindrical shapes. The refractive index is an intrin-

sic measure of the cell content and also defines how light interacts with tissues. Dendrites are the principal recipients of incoming chemical messengers from axon terminals. On dendritic shafts, specialized structural elements (*dendritic spines*) initially emerge as collateral filopodia then mature into spineous synaptic contacts, or filopodia are pruned. The mechanisms by which dendrogenesis leads to spine formation have not been resolved. Thus a label-free noninvasive method for imaging such structures in detail is very beneficial.

Figure 3 shows the SLIM image of a live rat hippocampal neuron in culture, i.e., immersed in culture medium during imaging. Following the routine applied to nanotubes, we retrieved the distance map of the axon [Fig. 3(b)] and its refractive index distribution. The average refractive index contrast obtained is $\Delta n = 0.034$. Thus, by using the refractive index of the culture medium of 1.34, we obtain an average value for the neuronal structure that is comparable with what has been measured before on other live cells [5]. Besides providing the absolute values for the refractive index of cellular structures, which is crucial for predicting the light-tissue interaction,

SLIM can quantify the spatial inhomogeneities of the neurite structures. Thus, the discrete regions of the enhanced refractive index are most likely related to the development of synaptic connections. The ability to image these dynamically without the need for fluorescence tagging may open the door for studying cell-to-cell communication.

In summary, we reported novel applications of SLIM that cross the boundary between biomedicine and nanoelectronics. We believe that here we reported for the first time the optical topography of graphene, which may provide a high-throughput alternative to testing such atomic-scale structures. We developed an approach for extracting the refractive index information from cylindrical structures. This procedure was applied successfully to SNTs and neurites. Based on these initial results, we anticipate that SLIM may become a useful quantitative tool in both materials science and cell biology.
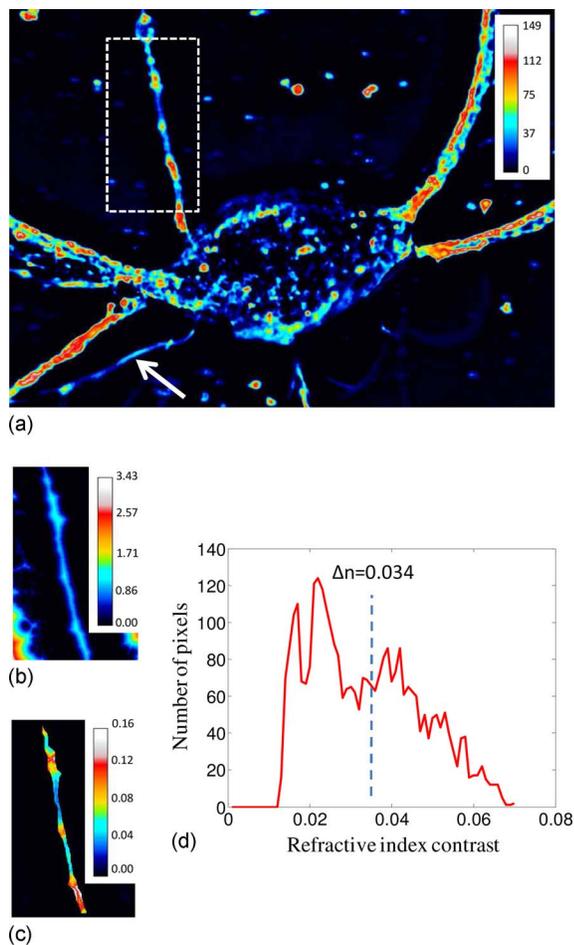
Fig. 3. (Color online) (a) Optical path-length map of a hippocampal neuron. Color bar has units of nanometers; (b) distance map of the axon selected in (a), in micrometers; (c) refractive index contrast map; (d) refractive index contrast histogram; the average value is indicated.

References

1. G. Popescu, in *Methods in Cell Biology*, P. J. Bhanu, ed. (Elsevier, 2008), p. 87.
2. C. Depeursinge, in *Digital Holography and Three-Dimensional Display*, T.-C. Poon, ed. (Springer, 2006), p. 98.
3. G. Popescu, T. Ikeda, K. Goda, C. A. Best-Popescu, M. Laposata, S. Manley, R. R. Dasari, K. Badizadegan, and M. S. Feld, Phys. Rev. Lett. **97**, 218101 (2006).
4. D. Zicha and G. A. Dunn, J. Microsc. **179**, 11 (1995).
5. N. Lue, G. Popescu, T. Ikeda, R. R. Dasari, K. Badizadegan, and M. S. Feld, Opt. Lett. **31**, 2759 (2006).
6. Z. Wang, L. J. Millet, M. U. Gillette, and G. Popescu, Opt. Lett. **33**, 1270 (2008).
7. H. Ding, Z. Wang, F. Nguyen, S. A. Boppart, and G. Popescu, Phys. Rev. Lett. **101**, 238102 (2008).
8. Z. Wang, L. J. Millet, H. Ding, M. Mir, S. Unarunotai, J. A. Rogers, M. U. Gillette, and G. Popescu, "Spatial light interference microscopy (SLIM)" Nat. Methods, submitted for publication.
9. F. Zernike, Science **121**, 345 (1955).
10. K. S. Novoselov, A. K. Geim, S. V. Morozov, D. Jiang, Y. Zhang, S. V. Dubonos, I. V. Grigorieva, and A. A. Firsov, Science **306**, 666 (2004).
11. P. Blake, E. W. Hill, A. H. C. Neto, K. S. Novoselov, D. Jiang, R. Yang, T. J. Booth, and A. K. Geim, Appl. Phys. Lett. **91**, 063124 (2007).
12. M. Ishigami, J. H. Chen, W. G. Cullen, M. S. Fuhrer, and E. D. Williams, Nano Lett. **7**, 1643 (2007).
13. A. Shukla, R. Kumar, J. Mazher, and A. Balan, Solid State Commun. **149**, 718 (2009).
14. I. S. Chun and X. L. Li, IEEE Trans. Nanotechnol. **7**, 493 (2008).
15. T. Kipp, H. Welsch, C. Strelow, C. Heyn, and D. Heitmann, Phys. Rev. Lett. **96**, 077403 (2006).